Localization phase diagram for a disordered system in a magnetic field in two dimensions

1993 J. Phys.: Condens. Matter 5 6043

(http://iopscience.iop.org/0953-8984/5/33/013)

J. Phys.: Condens. Matter 5 (1993) 6043–6054. Printed in the UK

Localization phase diagram for a disordered system in a magnetic field in two dimensions

M Bockstedte† and S F Fischer

Physik Department T38, TU München, D-85747 Garching, Federal Republic of Germany

Received 4 June 1993

Abstract. A phase diagram for the localization–delocalization transition of a two-dimensional disordered semiconducting system in a perpendicular magnetic field B is investigated with a numerical method. Disorder originates from a random distribution of shallow impurities, measured in units of the impurity concentration c. Starting with a tight-binding Hamiltonian and an impurity state basis, the localization criterion is defined by means of the quantum connectivity of impurities. Finite-size scaling is employed to study the transition in the B–c parameter space. On this footing a phase diagram of the localization–delocalization transition in the B–c parameter space is calculated. At low concentrations $c < c_1 \approx 0.246a^{-2}$, where a is the impurity radius, all states are localized. Above c_1 two nose-shaped areas of a phase of delocalized states exist, the tips of which are found at $(c_1, B_1) = (0.246 \pm 0.004a^{-2}, 0.013 \pm 0.001)$ and $(c_3, B_3) = (0.67 \pm 0.03a^{-2}, 0.76 \pm 0.07)$ with the magnetic field given in terms of a^2l^{-2}, where l is the Lamor length. Both areas join at $(c_2, B_2) = (1.2 \pm 0.2a^{-2}, 0.233 \pm 0.009)$. States are well localized at $B = 0$. An estimate of the localization length exponent is given. The transition is discussed in terms of orbital shrinking and interference effects, which are safely distinguished. The latter mechanism can account for a re-entrant behaviour with respect to the magnetic field. The metal–insulator transition is discussed as a function of the electron density in conjunction with the phase diagram. Results are compared with previous calculations within the zero differential overlap approximation.

1. Introduction

The metal–insulator transition (MIT) is discussed in the zero-temperature limit under two aspects, namely a transition due to many-particle correlation effects known as the Mott–Hubbard transition (e.g. Mott 1980) and as a localization–delocalization transition (LDT) first investigated by Anderson (1958). The occurrence of the LDT in three-dimensional systems and its absence in one-dimensional systems is well understood, but the situation is more complex in two dimensions. Analytical work (Abrahams *et al* 1979, Wegner 1989) as well as numerical studies (MacKinnon and Kramer 1983) have established that in two dimensions all states are localized in the absence of a magnetic field and spin–orbit scattering. On the other hand there are good reasons for an LDT to occur in the presence of a magnetic field or spin–orbit scattering, since both have influence on the localizing destructive interference due to backscattering. In this context, one-particle tight-binding models are studied numerically. Diagonal disorder is commonly introduced into these models by distributing the site energies according to a distribution function (Anderson model).

† Present address: Fritz-Haber-Institut der Max-Planck-Gesellschaft, Faradayweg 4-6, D-14195 Berlin, Federal Republic of Germany.

0953-8984/93/336043+12$07.50

In this paper we study numerically the LDT of a two-dimensional disordered system in a magnetic field. Our model Hamiltonian contains purely off-diagonal disorder which, in contrast to the Anderson model, originates from randomly distributed impurities. The impurity concentration thus becomes a measure of the disorder. Such a model for the LDT in two-dimensional systems might be applicable to δ-layer structures grown in semiconductors where magnetotransport has been studied by several groups recently (Ye 1990 and references therein). Such systems have been investigated in the low-temperature (~ 4 K) and low-concentration regime ($< 10^{11}$ cm^{-2}), where hopping transport is relevant. This limit is well described by current theories (Schirmacher 1990, Shkolovskii and Efros 1984). For the high-concentration limit ($> 10^{12}$ cm^{-2}) subband quantization has been observed (Zrenner 1985).

We will be concerned with the intermediate regime, where the question of an MIT is still open. As in a preceding paper (Gammel and Fischer 1991) we investigate the LDT in a finite-size scaling approach now avoiding the zero-differential overlap approximation, which has a substantial effect on the phase diagram in the B–c parameter space. The localization criterion is formulated in terms of the quantum connectivity first considered by Root *et al* (1988). We investigate the phase boundary using the phenomenological renormalization group technique (Nightingale 1976). The phase diagram is qualitatively discussed in terms of the relevant mechanisms contributing to the LDT. The MIT is discussed as a function of the electron density in conjunction with the phase diagram. The paper is divided into three sections. In section 2 we develop the model and reviewed the method. In section 3 the results are presented. Section 4 contains a summary and conclusion.

2. The model and method

The physical system under consideration consists of shallow impurities disposed in an otherwise periodic semiconducting material to form a δ-layer geometry. The impurities are distributed at random on a two-dimensional mesh of length L according to a concentration c. Perpendicular to it a homogeneous magnetic field B is established. The mesh confines the impurity positions to its sites, thus avoiding clustering. The mesh width $A_{\text{grid}} = 1/50\sqrt{c}$ is of the same magnitude as the lattice constant of the host material, when concentrations $c \leqslant a^{-2}$ are considered.

The concentration regime of interest for the appearance of the metal–insulator transition is below $c \sim a^{-2}$ where the average neighbour distance approaches the Bohr radius a of an impurity state and above the low concentration hopping regime of about $c \sim 0.1\,a^{-2}$. The system is treated in the effective medium approach. Starting from a basis of impurity states we obtain within the tight-binding one-electron approximation the following eigenvalue equation

$$\sum_{\tilde{\nu}}\left(\epsilon_\nu \delta_{\nu\tilde{\nu}} + \sum_{\kappa\neq\tilde{\nu},\nu\neq\tilde{\nu}} \langle\nu|V_\kappa(\boldsymbol{r})|\tilde{\nu}\rangle\right) c_{\tilde{\nu}} = \epsilon \sum_{\tilde{\nu}} \langle\nu|\tilde{\nu}\rangle\, c_{\tilde{\nu}} \tag{1}$$

where $|\nu\rangle$ is an impurity state located at $\boldsymbol{r}_\nu$ in the presence of a perpendicular magnetic field. The diagonal term ϵ_ν represents the site energy of the impurity, whereas $\langle\nu|V_\kappa|\tilde{\nu}\rangle$ is the potential matrix element of the impurity states $|\nu\rangle$ and $|\tilde{\nu}\rangle$ at $\boldsymbol{r}_\nu$ and $\boldsymbol{r}_{\tilde{\nu}}$ respectively of the potential contribution of the impurity at $\boldsymbol{r}_\kappa$. In contrast to the Anderson model the site energy ϵ_ν is kept fixed for all impurities. Periodic boundary conditions are applied via the minimum image convention (Aoki 1977).

In (1) we neglected off-diagonal kinetic energy matrix elements $\langle\nu|(1/2m^*)[\hat{p}+(e/c)A)]^2|\tilde{\nu}\rangle$, $\nu \neq \tilde{\nu}$ and the sum $\sum_{\kappa\neq\nu}\langle\nu|V_\kappa|\nu\rangle$. The contribution of the kinetic energy term is small as long as $c < a^{-2}$ applies and B is below the high field limit. The potential term is only small when $c \leqslant 0.3\,a^{-2}$ holds. In general it causes additional diagonal disorder. Its role will be discussed in section 3.

The potential of a shallow impurity is well described by a Coulomb potential in the effective medium approximation, but with a magnetic field present there is no closed form at hand. Only asymptotic expressions for the ground-state wavefunctions $\Psi_\kappa(r)$ are available in some limiting cases (Shkolovskii and Efros 1984), $l \gg a$ and $l \ll a$ with the Lamor length l, which are of significance in the theory of hopping conduction. However, this leaves us with the problem of obtaining expressions for $r \sim a$ and in the physically crucial case $l \sim a$. In order to circumvent these obstacles inevitably faced with most potentials, we proceed with a simple but neat approach. The impurity state is described in a harmonic approximation of the impurity potential.

We then evaluate potential matrix elements consistently assuming a short-range potential (see below). The frequency of the oscillator is chosen to yield the zero-field impurity radius a:

$$\omega_0 = \frac{\hbar}{m^* a}. \tag{2}$$

The orbitals of an impurity at r_κ are given in terms of an impurity at the origin by

$$\Psi_\kappa(r) = \exp\left(\frac{\mathrm{i}}{2l^2}(r \times r_\kappa)\cdot e_z\right)\Psi_0(r - r_\kappa) \tag{3}$$

where the cyclic gauge has been used. The xy plane of the coordinate system coincides with the δ-layer and $B = Be_z$. Within the harmonic approximation the impurity state is separable. The electronic motion perpendicular to the xy plane is given by a one-dimensional oscillator while the magnetic field only has influence on motion in the plane. We restrict ourselves to a single-band approximation considering only ground-state orbitals

$$\Psi_0(r) = \frac{1}{\sqrt{\pi}\tilde{a}}\exp\left(-\frac{(x^2+y^2)}{2\tilde{a}^2}\right)\zeta(z) \tag{4}$$

with $\tilde{a} = a(1+\frac{1}{4}a^4l^{-4})^{-1/2}$ and $\zeta(z)$ is the ground state of the one-dimensional oscillator. The asymptotic form of $\Psi(r)$ certainly decays faster than the asymptotic exponential behaviour found at $l \gg a$ for shallow impurities. But since the transition is expected at concentrations higher than $0.1\,a^{-2}$ the basic results of our model should apply at least qualitatively, also for a more realistic potential. As the impurity Hamiltonian is separable and as the impurities are confined to the xy plane, $\zeta(z)$ is independent of r_ν when Ψ_0 in (4) is substituted into (3) and integrals over $\zeta(z)$ either do not contribute to (1) or can be eliminated by shifting the energy scale.

The overlap matrix element and the site energy are given respectively by

$$\langle\nu|\tilde{\nu}\rangle = \exp\left[-\frac{(r_\nu - r_{\tilde{\nu}})^2}{4\tilde{a}^2}\left(1+\frac{\tilde{a}^4}{4l^4}\right)\right]\exp\left(\frac{\mathrm{i}}{2l^2}(r_\nu \times r_{\tilde{\nu}})\cdot e_z\right) \tag{5}$$

and

$$E_K = \hbar\Omega \tag{6}$$

with $\Omega = \omega_0(1 + \frac{1}{4}a^4l^{-4})^{1/2}$. The matrix element $\langle\nu|V_\kappa|\tilde{\nu}\rangle$ has to be calculated beyond a harmonic approximation. This is done in correspondence with a δ-like shape of the potential, as was done by Gammel and Fischer (1991):

$$\langle\nu|V_\kappa(r)|\tilde{\nu}\rangle = V_0 \exp\left(-\frac{1}{2\tilde{a}^2}[(r_\kappa - r_\nu)^2 + (r_\kappa - r_{\tilde{\nu}})^2]\right) \exp\left(\frac{\mathrm{i}}{l^2}[r_\kappa \times (r_{\tilde{\nu}} - r_\nu)] \cdot e_z\right) \quad (7)$$

with $V_0 = \frac{1}{2}\hbar\omega_0^2/\Omega$. The value of V_0 is chosen such that the potential expectation value $\langle\nu|V_\nu|\nu\rangle$ in the harmonic approximation is given by (7).

Measuring energies in units of $\hbar\omega_0$ one obtains $\epsilon_\kappa = (1 + \frac{1}{4}a^4l^{-4})^{1/2}$ and $V_0 = \frac{1}{2}(1 + \frac{1}{4}a^4l^{-4})^{-1/2}$. We shall use the impurity radius as a length scale and note that only ratios of $a^2\tilde{a}^{-2} = (1 + \frac{1}{4}a^4l^{-4})^{-1/4}$ and a^2l^{-2} appear in (5) and (7). Since only a^2l^{-2} is affected by the magnetic field, which is proportional to it, we take this ratio as a measure of B. This way the phase diagram becomes independent of the impurity radius. The mass m^* is not important as it merely determines the energy scale, which is of little relevance here.

The criterion for localization of states involves the transition probability between two impurity states given by

$$P_{ij} = \lim_{\eta\to\infty} \left| \int\int \mathrm{d}^3r\,\mathrm{d}^3\tilde{r}\; \Psi_j^*(r) G(r, t, \tilde{r}, \tilde{t}) \Psi_i(\tilde{r}) \right|^2 \quad (8)$$

with the initial and final states ψ_i and ψ_j respectively, and the retarded Green function

$$G(r, t, \tilde{r}, \tilde{t}) = -\mathrm{i}\theta(t - \tilde{t}) \sum_\nu \Phi_\nu(\tilde{r})\Phi_\nu^*(r) \exp\left(-\frac{\mathrm{i}}{\hbar}E_\nu(t - \tilde{t})\right). \quad (9)$$

Taking the limit of (8) yields (Root *et al* 1988, Gammel and Fischer 1991)

$$P_{ij} = \sum_\nu |\langle i|\nu\rangle|^2 |\langle j|\nu\rangle|^2. \quad (10)$$

Following Root *et al* (1988) we introduce the quantum connectivity

$$\Delta_{ij} = \frac{P_{ij}}{\sqrt{P_{ii}P_{jj}}}. \quad (11)$$

This quantity will be used in analysing the degree of localization of the states by means of finite-size scaling. If all states were localized the quantum connectivity Δ_{ij} should decay with increasing distance between the impurities at r_i and r_j. On the other hand with delocalized states existing Δ_{ij} should not show any specific asymptotic behaviour. We introduce a localization length as a function of the concentration and the magnetic field by evaluating the second moment of the distribution of the Δ_{ij}:

$$\xi_L^2 = \left\langle \frac{\sum_{ij}(r_i - r_j)^2\Delta_{ij}}{\sum_{ij}\Delta_{ij}} \right\rangle. \quad (12)$$

Here the angular brackets denote a configurational average. We also define an energy-dependent quantity by restricting the summation over ν_ϵ in (9) and (10) on finite energy intervals or a single energy ϵ. Then the energy-dependent transition probability is given by

$$P_{ij}^\epsilon = \sum_{\nu_\epsilon} |\langle i|\nu_\epsilon\rangle|^2 |\langle j|\nu_\epsilon\rangle|^2.$$

The energy-dependent quantum connectivity is defined according to (11) by

$$\Delta_{ij}^{\epsilon} = \frac{P_{ij}^{\epsilon}}{\sqrt{P_{ii}P_{jj}}}. \tag{13}$$

The corresponding localization length is obtained by (12) using (13) instead of (11). The localization length thus defined is smaller than the system size L. Therefore, whenever delocalized states begin to appear in the finite system, one expects that

$$\xi_L \sim L$$

whereas the constant factor may depend on the other physical parameters. If the states are localized the size dependence of ξ_L will be weak, provided the size of the system is large enough. We assume that at the transition point of the LDT the localization length of the infinite system diverges according to a power law

$$\xi \sim |K - K_C|^{-\nu}$$

where the parameter K may describe the amount of disorder (Fastenrath 1990, MacKinnon and Kramer 1983) or a physical parameter like the magnetic field or the energy (Huckestein and Kramer 1990). Instead of investigating the finite-size scaling directly as has been done by various authors for other models (Fastenrath 1991, Huckestein 1990), we approximate the transition points using the Nightingale phenomenological renormalization group (PRG) equation

$$\Xi_L = \frac{\xi_L(K)}{L} = \frac{\xi_{L'}(\tilde{K})}{L'} = \Xi_{L'} \tag{14}$$

where Ξ_L is the renormalized localization length, which is an appropriate scaling variable, as has been shown by MacKinnon and Kramer (1983) for the two- and three-dimensional Anderson model and by Ohtsuki *et al* (1992) for a three-dimensional system in a strong magnetic field. The PRG equation is a direct consequence of the finite-size scaling hypothesis (Barber 1983). The fixed point $K^*_{L,L'}$ for different system sizes L and L' given by (14) is an estimate for the transition point K^*. With increasing system size L and L' the fixed point converges to the transition point. An estimate of the localization length exponent ν is obtained by expansion to first order of ξ_L around K^* and the fact that $(\partial^i/\partial K^i)\xi_L \sim L^{1+i/\nu}$ holds:

$$\nu = \log\frac{L}{L'}\,\log\left(\left.\frac{\partial\,\Xi_L}{\partial K}\right|_{K_C} \Big/ \left.\frac{\partial\,\Xi_{L'}}{\partial K}\right|_{K_C}\right)^{-1}. \tag{15}$$

The parameter K needs a physical identification. The LDT will be investigated as a function of the disorder parameter concentration and the magnetic field B. We choose K to represent a parameter characterizing lines $(c(K), B(K))$ in the c–B parameter space. Fixed points K^* of (14) are found therefore where those lines $(c(K), B(K))$ intersect the phase boundary.

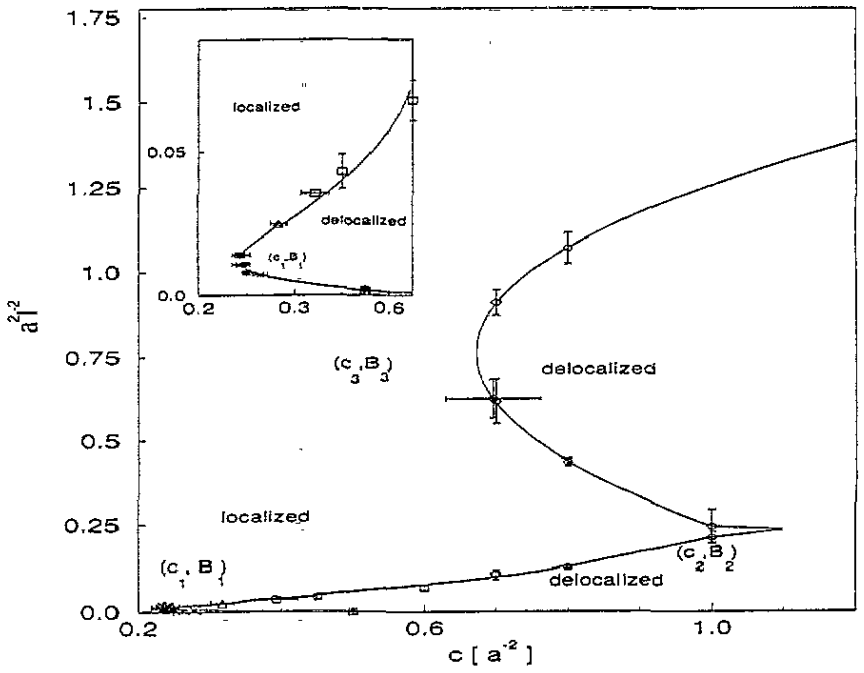

Figure 1. Phase diagram of the LDT of the system described by (1). The inset is a magnification of the part for $c < 0.6a^{-2}$—$P_1 = (c_1, B_1)$, $P_2 = (c_2, B_2)$ and $P_3 = (c_3, B_3)$. Fixed points $(c^*_{L,L'}, B^*_{L,L'})$ are presented with error bars (o: $L = 15, L' = 16$; ◇: $L = 18, L' = 19$; □: $L = 18, L' = 20$; Δ: $L = 20, L' = 22$; ∗: $L = 25, L' = 27$; •: $L = 29, L' = 33$).

3. Results

A phase diagram for the LDT has been calculated employing the method described before. The localization length ξ_L has been computed up to an accuracy of 4×10^{-3} for system sizes from $L = 15a$ up to $33a$. The fixed points are obtained from (14) with an accuracy of about 10%. The error of the fixed points at higher fields is larger. At magnetic fields with $a^2/l^2 \sim 1$ the statistical fluctuations of ξ_L are not small, since extended states are mainly found in the high-energy tails of the density of states. Time-consuming averaging over more than four times as many samples helps, but the accuracy of the fixed points suffers. The resulting transition points $(c^*_{L,L'}, B^*_{L,L'})$ obtained are thus shown with error bars in figure 1. The phase boundary is represented by the full curve and is obtained by piecewise polynomial fit of the fixed points, its smoothness and steadiness being assumed.

The phase diagram contains several interesting features. First of all there are two nose-shaped areas of extended states. These areas join at the point $(c_2, B_2) = (1.2 \pm 0.2a^{-2}, 0.233 \pm 0.009)$. The tips of the noses are found at the points $(c_1, B_1) = (0.246 \pm 0.004a^{-2}, 0.013 \pm 0.001)$ and $(c_3, B_3) = (0.67 \pm 0.03a^{-2}, 0.76 \pm 0.07)$ in the phase diagram. The remainder of the parameter plane contains a phase of localized states. Second, there are no extended states found at $B = 0$. However the phase boundary seems to approach $B = 0$ with increasing impurity concentration. In contrast to models with purely off-diagonal disorder, showing indication for an LDT even at $B = 0$ (Debeney 1976 and Odagaki 1980), the disorder seems to be strong enough here to provide a short extension of wavefunctions.

In order to estimate the localization length exponent, we evaluate the localization length

as a function of the concentration at (c_1, B_1). Data of ξ_L of four different system sizes $L = 25a$, $27a$, $29a$ and $33a$ are used with an accuracy of at least 4×10^{-3}. The localization length data are fitted to polynomials with maximum degree of five. The fixed point itself and the slope of the localization length are calculated from these polynomials. The data and fitted curves are presented in figure 2. In table 1 the fixed points $c^*_{L,L'}$ and the exponents $\nu_{L,L'}$ obtained by (15) are given.

Table 1. Fixed-point $c^*_{L,L'}$ and $\nu_{L,L'}$ for different L and L' at $a^2l^{-2} = 0.01$.

$L\,(a)$	$L'\,(a)$	$c^*_{LL'}\,(a^{-2})$	$\nu_{LL'}$
33	29	0.248 ± 0.002	1.2 ± 0.5
33	27	0.250 ± 0.002	0.73 ± 0.05
33	25	0.243 ± 0.003	0.52 ± 0.1
29	27	0.251 ± 0.003	0.44 ± 0.06
29	25	0.241 ± 0.004	0.43 ± 0.05
27	25	0.236 ± 0.005	0.39 ± 0.06

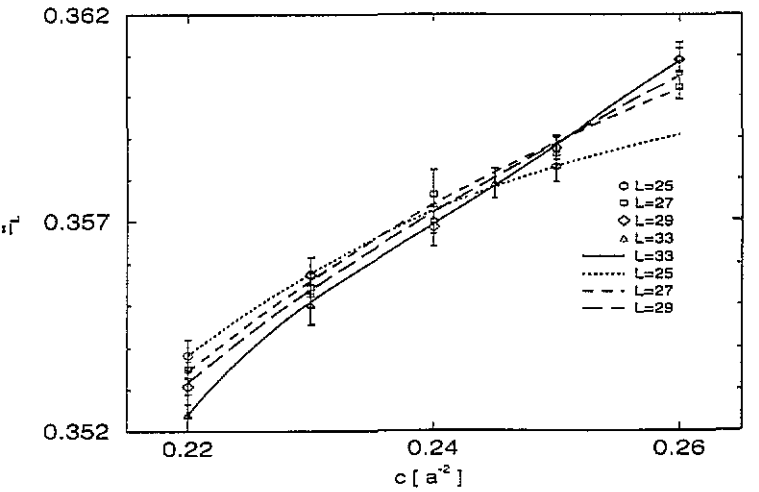

Figure 2. Renormalized localization length Ξ_L against c for $B = 0.01$ and different system sizes L.

Deviations of $c^*_{L,L'}$ for different system sizes are small except for the values for $L = 25a$. The exponent $\nu_{L,L'}$ is still increasing with system size and has not converged. To get a reliable value larger systems have to be taken into consideration. The exponent $\nu_{29,33} = 1.2 \pm 0.5$ may be taken as a first approximation and deviations from this value are expected to lie within the error bar. Chang *et al* (1990) have shown for the Anderson model with a Gaussian distribution of site energies that the estimate of the critical disorder obtained by the same method coincide with those obtained by other methods (Bulka *et al* 1987). Nevertheless their localization length exponent has not converged either. Our estimate $\nu_{29,33}$ obeys $\nu_{29,33} > 1$ and hence fulfills the Harris criterion (Chayes *et al* 1986) $\nu > 2/d$ in two dimensions: $d = 2$. Huckestein (1990) calculated the localization length exponent in the limit of a high magnetic field and a white noise potential and has found

$\nu = 2.34 \pm 0.04$. Whether or not our exponent should coincide with theirs cannot be said definitely. It is more likely that the exponents are different, since in our case the magnetic field is quite small and the magnetic length scale is of the same magnitude as the potential length scale. A breakdown of the one-parameter finite-size scaling reported by Aoki and Ando (1985) in the quantum Hall regime is not observed in our system. In the light of the poor statistics and the insufficient information about ν at (c_1, B_1) it seems to be impossible to determine the localization length exponent at (c_3, B_3), where $l \sim a$, in a meaningful way.

During the discussion of the basis set we already mentioned two limiting cases for the magnetic field dependence of the impurity state. The question arises if simple interpretations of the LDT can be found for these limits. In this context it is informative to investigate the phase boundary as a function of the model parameters and to incorporate length scales. Since all quantities of the phase diagram can be scaled by the impurity radius, the shape of the phase boundary becomes independent of other parameters.

The magnetic-field-dependent length l and $\tilde{a}$ affect the matrix elements (5) and (7) in different ways. The Lamor length which enters at the phase factor and the field-dependent impurity radius $\tilde{a}$ causes orbital shrinking. The field dependence of $\tilde{a}$ is low as long as $l \gg a$, for $|a^2 - \tilde{a}^2| < 0.01a^2$ holds, and becomes significant when $l \leqslant a$. Setting $\bar{l} = l/\sqrt{2}$ in the phase factors of (5) and (7) and evaluating some of the fixed points we find that those fixed points $\bar{B}^*_{L,L'}$ with $l > a$ scale within the numerical error as $\bar{B}^*_{L,L'} \approx \frac{1}{2}B^*_{L,L'}$ and those with $l \leqslant a$ remain unchanged $\bar{B}^*_{L,L'} \approx B^*_{L,L'}$. Hence the LDT occurring at small magnetic field, i.e. $l > a$, is related to interference effects alone. The destruction of interference by the magnetic field is thus a destruction of weak localization. The localization of states at higher magnetic fields $l \leqslant a$ is due to orbital shrinking.

Surprisingly, interference effects can account for a re-entrant phase transition with respect to the magnetic field alone. The reason may be found in the behaviour of the potential matrix elements (7) of the states. The absolute value of the potential matrix elements of the impurity decreases with increasing magnetic field due to interferences in the sum (7). The absolute values $|V_{ij}|$ are distributed between an upper and lower bound, the impurity distance r_{ij} kept fixed as depicted in figure 3. For example, shifting B from 0.018 to 0.56, $c = 0.8a^{-2}$ with $r_{ij} = 2a$, decreases the lower and upper bound about $1/6\hbar\omega_0$, though V_0 is only diminished by about one per cent. The decreasing $|V_{ij}|$ favours localization, as for $V_{ij} = 0$ no extended states are found in this concentration regime. In contrast to this effect the distribution of the phases of the potential coupling and the overlap covers an increasing interval with increasing magnetic fields for fixed r_{ij}. For short distances r_{ij} this interval is small, as can be seen from (5) and (7). This effect induces delocalization, since delocalized states appear at finite but small B at first where the bounds on $|V_{ij}|$ do not bear a significant field dependence.

The phase diagram presented in figure 1 separates areas where all states are localized and those where delocalized states are present. At the phase boundary at least one state begins to percolate the system. However, the system cannot be said to be metallic unless states are delocalized at the Fermi level. Knowledge of the position of the mobility edges and of the Fermi level is therefore essential, in order to draw conclusions from the phase diagram regarding the MIT. Besides the magnetic field and the impurity concentration we have to consider the electron density as a further parameter which affects the position of the Fermi level. According to our model this is done by neglecting spin and excluding screening effects or many-particle interactions from the discussion.

The mobility edges are investigated employing the energy-dependent localization length ξ^ϵ_L; ξ^ϵ_L is computed over finite energy ranges instead of evaluating it at a single energy to

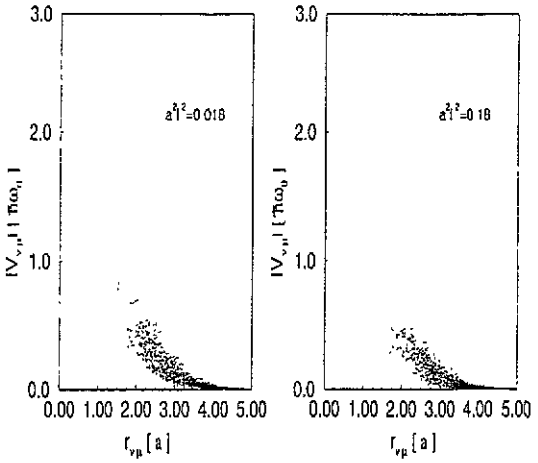

Figure 3. Absolute value of $\sum_{\kappa\neq\nu}\langle\nu|V_\kappa|\tilde{\nu}\rangle$ against $r_{\nu\tilde{\nu}}$ for $B = 0.018$ and $B = 0.18$ and $c = 0.8a^{-2}$.

avoid time-consuming averaging. We can estimate the position of the mobility edges within the width of the energy intervals. The width of the intervals is chosen smaller than $\hbar\Omega$.

The mobility band opens abruptly to its full width at the phase boundary. The band width is constant with respect to B within the nose at (c_1, B_1) but widens with increasing concentration, while the band edges slightly shift to higher energies. The density of states and the mobility edges are depicted in figure 4 for $c = 0.5\,a^{-2}$ and $B = 0.024$. Within the nose at (c_3, B_3) the lower band edge is positioned just above the centre of the density of state. The mobility band extends throughout the tail. A reliable estimate of the position of the upper band edge cannot be given due to fluctuations of the localization length ξ_L^ε at the tail of the density of states. It seems, though, that almost all states are delocalized beyond the lower mobility edge.

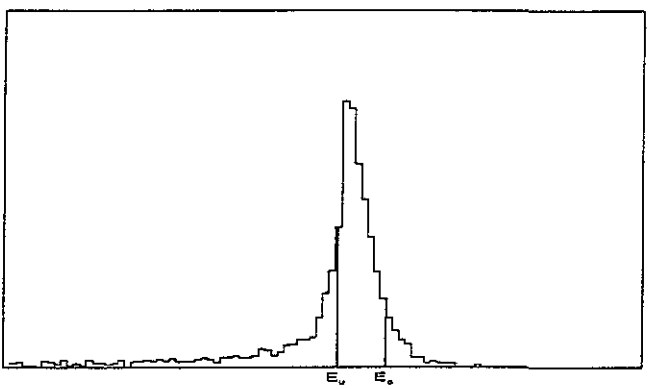

Figure 4. Density of states for $c = 0.5a^{-2}$ and $B = 0.025$. States between E_u and E_o are delocalized. The position of the mobility edges are $E_u \sim 0.7\hbar\omega_0$ and $E_o \sim 2.9\hbar\omega_0$.

The position of the Fermi level is easily obtained as a function of the electron density at a point (c, B) by averaging over the sequence of eigenenergies and inverting it. When (c, B) belongs to the phase where delocalized states occur four different regimes of electron density can be distinguished. Consider a fixed concentration c and critical fields B_a and B_b, $B_a < B_b$, belonging to the nose at (c_1, B_1). For magnetic fields B, with $B_a \leqslant B \leqslant B_b$, delocalized states exist. Suppose that the mobility band width is constant with respect to B, if $B_a \leqslant B \leqslant B_b$. At the critical fields B_a and B_b the Fermi level coincides with the upper

and lower band edges for one of the four electron densities respectively. The situation is sketched in figure 5 for $c = 0.5a^{-2}$, $B_a \sim 0.0023$ and $B_b \sim 0.043$. The following four cases can then occur.

(i) $n_{el,1} < n_{el} < n_{el,2}$. States are delocalized at the Fermi level for magnetic fields B with $B_a \leqslant B \leqslant B_b$. An MIT occurs according to the transition points given by the phase boundary.

(ii) $n_{el,4} > n_{el} > n_{el,1}$. A critical field $B_c < B_b$ exists such that the Fermi level is within the mobility band for magnetic fields B with $B_a \leqslant B \leqslant B_c$. The MIT occurs at critical fields within the phase of delocalized states. B_c depends on n_{el} and approaches B_a with increasing n_{el}.

(iii) $n_{el,2} < n_{el} < n_{el,3}$. The same situation persists as in the previous case. An MIT is observed at B_c below B_b, but with B_c approaching B_b with increasing n_{el}.

(iv) $n_{el} > n_{el,3}$ and $n_{el} < n_{el,4}$. The Fermi level lies above or below the mobility band for B with $B_a \leqslant B \leqslant B_b$. Though an LDT occurs no MIT can be observed.

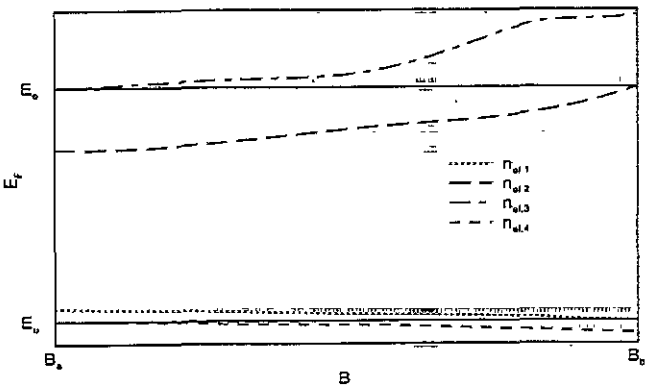

Figure 5. The Fermi level of the for electron densities $n_{el,i}$ (see text) against magnetic field. The full lines are the upper and lower mobility edge. The critical fields are B_a and B_b.

The magnetic field B_c and the four electron densities depend on the concentration.

Finally we discuss the influence of diagonal disorder on part of the phase diagram. The diagonal disorder introduced in this paper is correlated with the positions of the impurities. Diagonal disorder is thus achieved by replacing the site energy by

$$\epsilon_\nu = \hbar\Omega - \hbar\omega_0 \sum_\kappa \exp\left(-\frac{1}{2\tilde{a}^2}[(r_\kappa - r_\nu)^2 + (r_\kappa - r_\nu)^2]\right)$$

except for the prefactor $\hbar\omega_0$ this is just the sum $\sum_{\kappa\neq\nu}\langle\nu|V_\kappa|\nu\rangle$, which we omitted earlier. We computed the fixed points for $L = 18a$ and $L' = 20a$ in the regime of the nose at (c_1, B_1). This part of the phase diagram is shown in figure 6. It contains essentially the same features as the previous one shown in figure 1. The tip of the nose is found at $(c', B') = (0.238 \pm 0.04a^{-2}, 0.030 \pm 0.005)$ and lies at slightly higher fields than before. The shape of the phase boundary resembles that of the previous diagram, but the critical fields below B' lie higher than before.

In a preceding paper (Gammel and Fischer 1991) the same model has been investigated within the zero differential overlap approximation. For comparison the scale of the B axis of the phase diagram in figure 1 has to be rescaled by a factor of two in order to avoid an inconsistency of that paper.

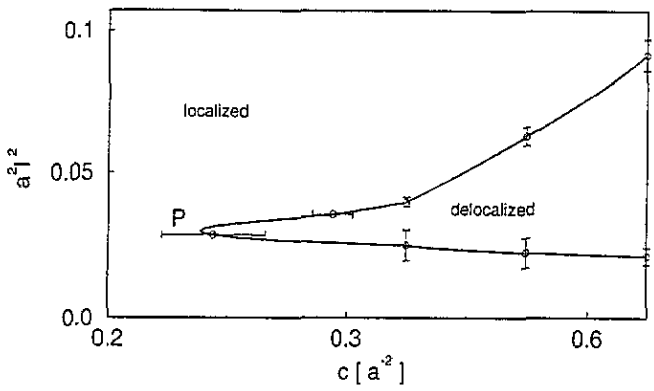

Figure 6. Phase diagram of the LDT of the system with additional diagonal disorder: $P = (c', B')$. Fixed points $(c^*_{L,L'}, B^*_{L,L'})$ are presented with error bars (o: L=18, L'=20).

The phase boundary shows similar features as those of the phase diagrams discussed here. There is only one nose shaped phase of delocalized states. The tip of the nose is located at $(c_{\min}, B_{\min}) \approx (1.6a^{-2}, 20\,\mathrm{kG})$—$20\,\mathrm{kG} \equiv 0.354$ in our units. The LDT occurs at considerably higher concentrations than that with the overlap included. We conclude that inclusion of the overlap has severe consequences on the shape of the phase boundary and is responsible for the existence of the two noses. This is different from studies of the LDT in three dimensions in the absence of magnetic fields (Bauer 1989, Ching and Huber 1982), where the neglect of the overlap had no major effect.

4. Summary and conclusion

In this paper we have investigated the MIT in a two-dimensional tight-binding model with off-diagonal disorder with a magnetic field B in a finite-size scaling approach. Disorder has been introduced by randomly distributed impurities and the impurity concentration c served as a measure of disorder.

A phase diagram of the LDT has been presented in the B–c parameter space. Two nose-shaped areas of delocalized states have been found, which join at the point (c_2, B_2). The tips of the noses are located at (c_1, B_1) and (c_3, B_3). At $B = 0$ only localized states have been found. Though the potential range has been short, we expect similar features of the phase boundary to occur for long-range potentials. The values of the c_i and B_i might depend on the potential range. However B_1 and B_3 should not change considerably, as is strongly suggested by our investigation of a similar model regarding potentials with Coulomb-like asymptotic behaviour (Bockstedte 1992).

Two mechanisms for the LDT have been explored. At high magnetic fields orbital shrinking has proven to localize all states, while interference effects give rise to a re-entrant LDT with respect to magnetic field. The latter have been discussed qualitatively in terms of a diminished absolute potential coupling between states due to destructive interference of the individual potential matrix elements and the behaviour of phase factors with increasing field (destruction of weak localization). The orbital shrinking effect is also present in the extended model mentioned above, which overcomes the restrictions of a tight-binding basis set.

We included the dependence of the Fermi level on the magnetic field, on the electron density, as well as the position of the mobility edges into our discussion of the MIT and found that an MIT occurs within the phase of delocalized states depending on a proper choice of the electron density.

Finally we wish to mention that our results could be relevant for the interpretation of the magnetoresistance data. Even though hopping motion between localized states also have to be considered, delocalized states always favour conduction. Thus we expect the sign of the magnetoresistance to change at the critical fields of the MIT. According to our phase diagram (figure 1) we predict the magnetoresistance to change its sign at magnetic fields $B \sim B_1$ and $B \sim B_3$. Thus two minima of the resistance with respect to the magnetic field should be observed due to a MIT for appropriate electron densities. Such a switch of sign has already been found in recent experiments (Ye 1989) at about $B \sim B_3$.

Acknowledgments

We wish to acknowledge many helpful discussions with B M Gammel.

References

Aoki H 1977 *J. Phys. C: Solid State Phys.* **10** 2583
Aoki H and Ando T 1985 *Phys. Rev. Lett.* **54** 831
Abrahams E, Anderson P W, Licardello D C and Ramakrishnan 1979 *Phys. Rev. Lett.* **42** 673
Bauer J D, Logovinsky V, Skinner J L 1989 *J. Chem. Phys.* **90** 2703
Bockstedte M 1992 *Diploma thesis* Technische Universität München
Bulka B, Schreiber M and Kramer B 1987 *Z. Phys.* B **66** 21
Chang T C, Bauer J D and Skinner J L 1990 *J. Chem. Phys.* **93** 8979
Chayes J T, Chayes L, Fisher D S, Spencer T 1986 *Phys. Rev. Lett.* **57** 2999
Ching W Y and Huber D L 1982 *Phys. Rev.* B **26** 5596
Debeney B T 1977 *J. Phys. C: Solid State Phys.* **10** 4719
Fastenrath U 1990 *Solid State Commun.* **76** 855
Fastenrath U, Adams G, Bundschuh R, Hermes T, Raab B, Schlosser I, Wehner T and Wichmann T 1991 *Physica* A **172** 302
Gammel B M and Fischer S F 1991 *Phys. Rev. Lett.* **66** 2919
Huckestein B 1990 *Physica* A **167** 175
Huckestein B and Kramer B 1990 *Phys. Rev. Lett.* **64** 1437
MacKinnon A and Kramer B 1983 *Z. Phys.* B **53** 1
Nightingale M P 1976 *Physica* A **83** 561
Odagaki T 1980 *Solid State Commun.* **33** 861
Ohtsuki T, Kramer B and Ono Y 1992 *Solid State Commun.* **81** 477
Root L J, Bauer J D and Skinner 1988 *Phys. Rev.* B **37** 5518
Schirmacher W 1990 *Phys. Rev.* B **41** 2461
Shklovskii B I and Efros A L 1984 *Electronic Properties of Doped Semiconductors (Springer Series in Solid State Science)* (Berlin: Springer)
Soukoulis C M, Zdetsis A D and Econoumou E N 1986 *Phys. Rev.* B **34** 2253
Wegner F 1989 *Nucl. Phys.* B **316** 663
Ye Qui-Yi, Shklovskii B I, Zrenner A, Koch F and Ploog K 1990 *Phys. Rev.* B **41** 8477
Ye Qui-Yi, Zrenner A, Koch F and Ploog K 1989 *Semicond. Sci. Technol.* **4** 500
Zrenner A, Reisinger H, Koch F and Ploog K 1985 *Proc. 17th Int. Conf. on Physics and Semiconductors, San Francisco* ed J D Chadi and W Harrison (Berlin: Springer)